Journal of Solid State Chemistry **157,** 134–143 (2001)
doi:10.1006/jssc.2000.9064, available online at http://www.idealibrary.com on IDEAL®

Characterization and Defect Structure of Anion-Excess Fluorite-Related Phases in *Ln*OF–LnF_3 Systems (*Ln* = Nd, Sm, Eu, Gd): From Isolated Defect Clustering to "Vernier" Modulated Phases

J. P. Laval,*,[1] A. Taoudi,* and A. Abaouz†

*Science des Procédés Céramiques et de Traitements de Surface, UMR-CNRS No. 6638, 123 Av. A. Thomas, 87060 Limoges Cedex France; and
†Laboratoire de Chimie Minérale Appliquée, Faculté des Sciences, B.P. 4010, Beni M'hamed, Meknès, Morocco

Received April 17, 2000; in revised form November 21, 2000; accepted December 8, 2000

The phases $LnO_{1-x}F_{1+2x}$, derived from the fluorite-type structure by anionic excess, form, for medium size *Ln* cations (*Ln* = Nd, Sm, Eu, Gd), a homogeneous series of orthorhombic symmetry (space group *Pmmn*, $a \approx b \approx a_F\sqrt{2}/2; c = a_F$). Structural comparison of these phases by X-ray powder diffraction allows us to make a better determination of their defect structure: O/F order in sheets perpendicular to the [001] axis and formation of 1:0:2 clusters which can be associated in dimer units. For Nd, an orthorhombic–tetragonal transition is explained by a change from 1:0:2 to denser 1:0:3 clusters. Comparison of the structural features of these phases with "vernier" modulated phases, isolated for Sm–Lu cations, allows a general classification of $LnO_{1-x}F_{1+2x}$ phases at low temperature to be proposed. All are characterized by the preservation of an anionic O/F order in sheets perpendicular to the $[001]_F$ axis and by a progressive loss of freedom in the accommodation of the anionic excess (nature and orientation of the clusters, tendency to long-range ordering) from La to Lu, caused by the decrease in *Ln* size and therefore in *Ln* coordination. © 2001 Academic Press

Key Words: **lanthanide oxyfluorides; defect structure; fluorite type; anionic clusters; anion-excess fluorite; vernier phases; modulated phases.**

INTRODUCTION

In *Ln*OF–LnF_3 subsystems, crystallochemical and structural characterization of phases is relatively sparse and often incomplete.

Three kinds of $LnO_{1-x}F_{1+2x}$ fluorite-related phases can be distinguished in the *Ln*OF–LnF_3 systems according to *Ln* size:

For large size *Ln* cations (La–Nd) (1–4), a tetragonal solid solution phase is formed ($a \approx a_F\sqrt{2}/2$, $c = a_F$; $P4/nmm$ space group), characterized by O/F ordering in sheets perpendicular to the [001] axis. Its structure, first studied by Zachariasen for its main feature (O/F order) (4), has since been reinvestigated by Laval *et al.* by means of a high-resolution neutron diffraction study of $LaO_{0.65}F_{1.70}$ (5) in order to determine the defect structure allowing the accommodation of the anionic excess. A second part to this work will describe the homologous phases in the systems with large size *Ln* cations (La, Ce, Pr).

For small and medium size *Ln* cations (Sm–Lu), an orthorhombic ($a \approx a_F$, $b \approx ma_F$, $c \approx a_F$) domain of "vernier phases," related to the fluorite structure by a one-dimensional process of anionic densification, has been isolated in a composition range increasing from Sm to Lu ($SmX_{2.16-2.19}$–$LuX_{2.11-2.22}$ or $X_{2.10-2.20}$ (6–14). The detailed structure of some members of the homologous series $Y_m(O, F)_{2m+1}$ has been determined (15–17). Moreover, a stoichiometric phase $Lu_3O_2F_5$, corresponding to the member $m = 3$ of the vernier series $Lu_m(O,F)_{2m+1}$, has been structurally described (12).

For *Ln* cations of medium size, the phase equilibria are more complex. Tanguy reported in the EuOF–EuF_3 system a narrow vernier domain $EuX_{2.16-2.19}$ coexisting with a monoclinic phase derived from fluorite type (18) with limits varying with temperature: $EuX_{2.30-2.35}$ at room temperature, $EuX_{2.21-2.35}$ at 500°C. Molyneux has shown the presence of a similar vernier domain in the SmOF–SmF_3 system (19) but described an apparent monoclinic distortion of the fluorite cell, closely related to the tetragonal cell reported by Zachariasen for $La(O,F)_{2+x}$, of limits $SmX_{2.30-2.40}$ at room temperature (19, 20). This phase becomes tetragonal at high temperature. De Kozak *et al.* in determining the phase diagram of the GdOF–GdF_3 system (21) have shown the presence of a fluorite-related phase, stable only at $T \geq 760$°C, but without indexing it. However, Roether, in his thesis work (11), had previously indexed an orthorhombic ($R2$) solid solution $GdX_{2.34-2.40}$ stable only at $T > 750$°C. He had also shown the presence of a similar orthorhombic phase at $T > 600$°C in the SmOF–SmF_3

[1]To whom correspondence should be addressed. E-mail: laval@unilim.fr.

0022-4596/01 $35.00

system, with the limits $SmX_{2.18-2.30.}$ and of a tetragonal phase at the same temperature range only for the composition $SmX_{2.168}$.

In the NdOF–NdF_3 system, only a tetragonal fluorite-related solid solution, similar to $LaO_{1-x}F_{1+2x}$, had been reported between $\sim$500 and 1000°C (22, 23).

Laval *et al.* (24) have refined the crystal structure of a powder sample of composition $SmO_{0.70}F_{1.60}$ in the orthorhombic system ($a \approx a_F\sqrt{2}/2$, $b \approx a_F\sqrt{2}/2$, $c \approx a_F$; *Pmmn* space group proposed by Roether) using a defect model derived from the defect structure described for the tetragonal $LaO_{0.65}F_{1.70}$ fluorite-related phase (5).

In the present work, we have undertaken a study of the homologous fluorite-related domains in the four systems $LnOF$–LnF_3 with Ln = Nd, Sm, Eu, Gd to determine precisely their composition limits at low temperature and their structural features.

PREPARATION AND PRELIMINARY STUDY OF THE ORTHORHOMBIC SOLID SOLUTIONS

(*a*) *Experimental*

The samples are prepared from dried ultrapure *Ln* oxides and fluorides by similar processes in Ni sealed tubes (Pt for Eu phases to avoid reduction to Eu^{2+}), involving one-day heating at 900°C, progressive decreasing in temperature to 500°C, and successive annealing at 500°C, 400°C, 300°C, 200°C, 100°C, and ambient temperature (one day annealing by temperature), after which the sample is water-quenched as fast as possible. After each annealing at a given temperature, the sample is crushed, measured by X-ray diffraction, and then sealed in a new nickel tube for the next annealing.

To determine whether repeated annealings lead to progressive hydrolysis and therefore to composition shifts, chemical analysis by pyrohydrolysis to Ln_2O_3 and measurement of the weight loss have been carried out on samples prepared with the same initial mixture and one or several successive cycles of thermal treatment. The composition shift after the first annealing can be estimated to be less than $< LnX_{0.005}$ and the total shift after several other cycles less than $< LnX_{0.01}$.

All the X-ray diffraction experiments are performed on a D5000 diffractometer equipped with a back-monochromator (Cu$K\alpha$ radiation). The limits of the solid solutions are determined on the X-ray diffraction patterns by detection of the neighboring phases of the Ln_2O_3–LnF_3 diagram, LnF_3 for the upper limit, $LnOF$ (rhombohedral or cubic variety) or vernier phases for the lower limits. All these last phases, although also structurally related to the fluorite type, have some diffraction peaks sufficiently different from those of the studied phases to be detected.

(*b*) *Results*

Solid solutions similar to the domain to which $SmO_{0.70}F_{1.60}$ belongs have been isolated in the four systems studied. Their limits of stability progressively change from one system to another and also with temperature and quenching speed.

In the NdOF–NdF_3 system, at $T > 400$°C, the tetragonal solid solution $NdO_{1-x}F_{1+2x}$ already known is obtained. Its lattice parameters resulting from samples water quenched from 600°C (Fig. 1 and Table 1) agree well with the values reported by Shinn and Eick (7) but not with those of Juneja *et al.* (22). At 600°C, its composition limits are $0.10 \leq x \leq 0.39$. At 400°C, a splitting of some diffraction peaks appears in a narrow domain about $x = 0.25$ in the middle of the previous solid solution, which corresponds to a slight orthorhombic distortion of the tetragonal solid solution, without distinguishable discontinuity of this solid solution. The new orthorhombic solid solution $NdO_{1-x}F_{1+2x}$, whose lattice parameters are very close to those of the tetragonal phase (Table 1 and Fig. 2a), extends to the entire fluorite-related domain at final temperatures lower than 400°C. Its composition limits are less extended than those of the tetragonal high-temperature domain. At 300°C, the limits are $0.18 \leq x \leq 0.35$ ($NdO_{0.82}F_{1.36}$–$NdO_{0.65}F_{1.70}$). They slightly decrease with decreasing annealing temperature (Fig. 1) and, at ambient temperature, they are $0.20 \leq x \leq 0.34$. The lattice parameters of samples that were slowly cooled to ambient temperature are also reported in Table 1. The orthorhombic–tetragonal transition is perfectly reversible with reheating of the samples. The lattice volume does not significantly change for a phase of the same composition annealed at various temperatures. That can explain why the orthorhombic–tetragonal transition seems to be progressive, without two-phase domains.

In the SmOF–SmF_3 system, some significant changes occur: the tetragonal solid solution does not appear below 900°C. The orthorhombic solid solution $SmO_{1-x}F_{1+2x}$ has been prepared pure in the limits $0.21 \leq x \leq 0.35$ at 500°C and its existence range strongly decreases to 0.30–0.33 after progressive decreasing to ambient temperature. Moreover, two other phases related to fluorite type can be prepared.

The first is a narrow orthorhombic domain, close to the limits of the previous phase at 500°C but not contiguous and well distinct at lower temperatures ($0.16 \leq x \leq 0.19$ at 500°C and at room temperature). It is characterized by some superlattice peaks and is structurally homologous to $Ln_m(O,F)_{2m+1}$ "vernier" phases, especially for Ln = Y and Lu.

The second is a new phase, also deriving from the fluorite-type structure, appearing for $T < 250$°C in a narrow range about $x = 0.33$–0.35. Even after annealings for several weeks, this new phase has always been obtained as a minor

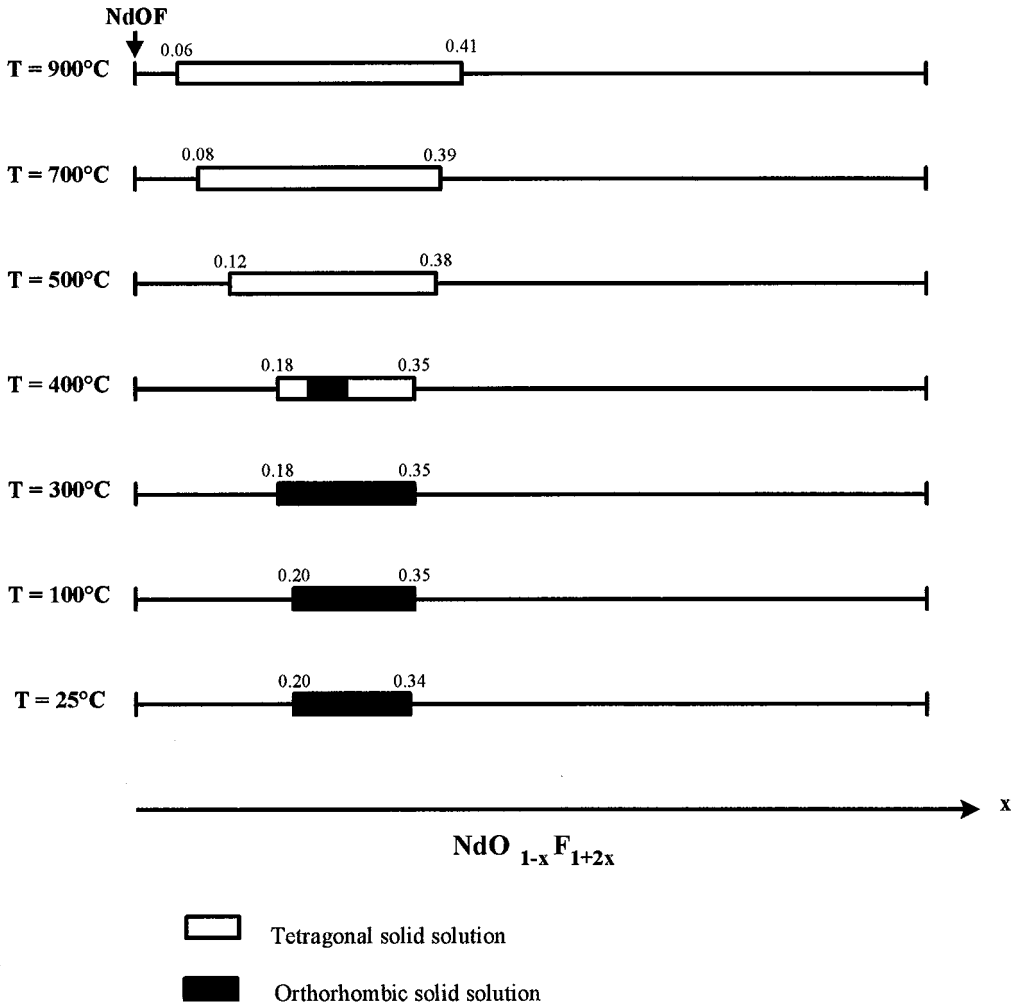

FIG. 1. Orthorhombic–Tetragonal transition and composition range in $NdO_{1-x}F_{1+2x}$ solid solution obtained by annealing and quenching at different temperatures.

phase, in the presence either of the orthorhombic $SmO_{0.667}F_{1.667}$ phase for $x = 0.33$–0.35 (Fig. 2b) or of the same orthorhombic phase plus SmF_3 for $x > 0.35$. Its exact composition is uncertain, owing to the failure to obtain a complete equilibrium. As this phase is very similar to the orthorhombic phase with a greater distortion of the fluorite lattice and a splitting of the main reflections, but almost the same cell volume ($V = 89.84$ Å^3 compared to 89.45 Å^3 for the orthorhombic phase $Sm(O,F)_{2.33}$), a severe overlapping of the diffraction peaks occurs. A complete summary of all its diffraction peaks appears unrealistic and the following indexing, based on a small number of clearly separated peaks, is only indicative: triclinic symmetry, $a = 3.923(2)$ Å, $b = 4.043(2)$ Å, $c = 5.665(3)$ Å, $\alpha = 90.52(2)^\circ$, $\beta = 90.50(2)^\circ$, $\gamma = 90.15(2)^\circ$. It corresponds to a distortion of the fluorite structure preserving the same orientation as the orthorhombic phase ($a \approx a_F\sqrt{2}/2$, $b \approx b_F\sqrt{2}/2$, $c = a_F$) and, because of the weakness of the diffraction peaks, it is not possible to determine whether extra lines, resulting from a long-range ordering process inside the fluorite-related structure, are present. Electron diffraction experiments fail to give information about this low-temperature variety which needs to be prepared by other ways.

In the $EuOF$–EuF_3 system, the monoclinic solid solution described by Tanguy *et al.* (18) can be indexed in the orthorhombic system with cell parameters reported in Table 1. This orthorhombic solid solution is stable down to ambient temperature by successive annealing and its limits correspond to those previously determined ($x = 0.30$–0.34 at room temperature compared to 0.30–0.35 from Ref. (18)). Moreover, for $T < 250$°C, extra lines of very low intensity can be observed after annealing for several days for $x = 0.34$–0.35. Their low intensity and the superposition of these lines with the ones characteristic of the $EuO_{1-x}F_{1+2x}$ orthorhombic solid solution have prevented the indexing of this new phase until now. It is very likely of the same type as

TABLE 1
Cell Parameters and Ratios for Some Compositions of the Orthorhombic $LnO_{1-x}F_{1+2x}$ Phases (Ln = Nd, Sm, Eu, and Gd)

		a (Å)	b (Å)	c (Å)	b-a	c/a	b/a
Nd	0.10(tet)	3.990(1)		5.690(1)		1.426	
	0.16(tet)	3.994(1)		5.698(1)		1.427	
	0.20(tet)	3.994(1)		5.701(1)		1.427	
	0.20	3.982(1)	4.019(1)	5.702(2)	0.037	1.432	1.009
	0.25(tet)	4.002(1)		5.705(2)		1.426	
	0.25	3.986(1)	4.023(1)	5.706(2)	0.037	1.432	1.009
	0.28	3.988(1)	4.024(1)	5.707(1)	0.036	1.431	1.009
	0.30(tet)	4.006(1)		5.710(2)		1.425	
	0.30	3.991(1)	4.025(1)	5.709(2)	0.034	1.431	1.009
	0.33(tet)	4.012(1)		5.715(2)		1.424	
	0.33	3.995(1)	4.028(1)	5.713(2)	0.033	1.430	1.008
	0.35(tet)	4.014(1)		5.714(2)		1.423	
	0.35	3.995(1)	4.030(1)	5.714(2)	0.035	1.430	1.009
	0.39(tet)	4.017(1)		5.714(2)		1.423	
Sm	0.30	3.902(2)	4.038(2)	5.642(3)	0.136	1.446	1.035
	0.33	3.910(1)	4.047(1)	5.653(2)	0.137	1.446	1.035
Eu	0.30 (Ref. (18))	3.881	3.998	5.598	0.117	1.442	1.030
	0.33	3.883(2)	4.023(2)	5.619(3)	0.140	1.447	1.036
	0.35 (Ref. (18))	3.881	4.030	5.623	0.149	1.449	1.038
Gd	0.33	3.862(1)	4.009(1)	5.592(2)	0.147	1.448	1.038

[a] For some Eu compositions, the cell parameters are recalculated from the monoclinic unit cell reported in Ref. (18).

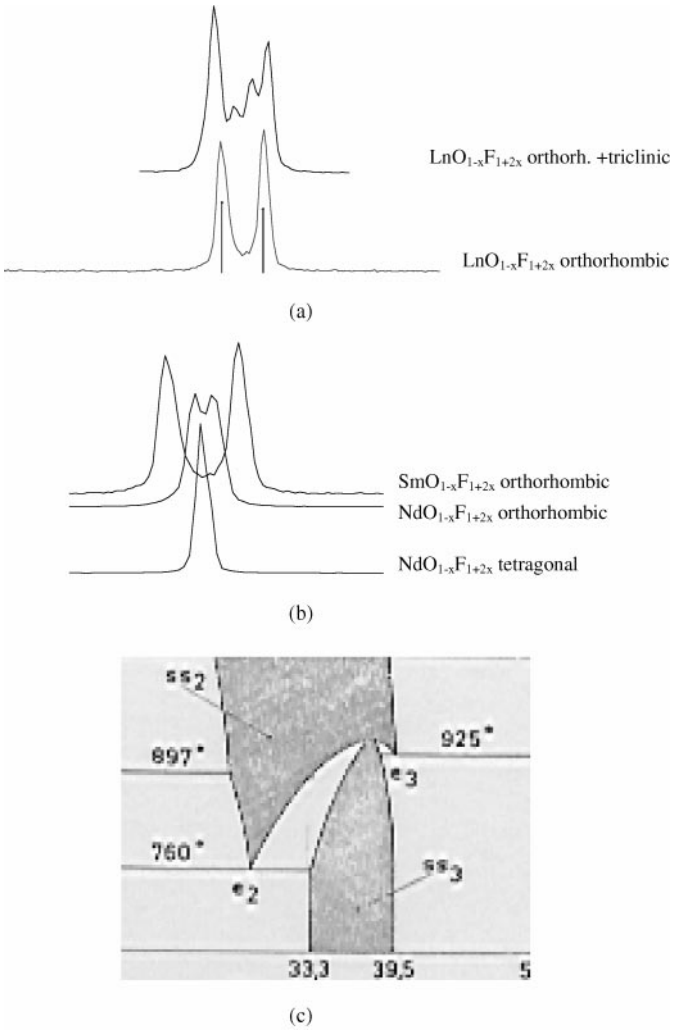

FIG. 2. (a) Comparison of homologous diffraction peaks (101) in tetragonal and (011) and (101) in orthorhombic $NdO_{1-x}F_{1+2x}$ and in $SmO_{1-x}F_{1+2x}$ (the 2θ scale is shifted to align the peaks). (b) Comparison of the same diffraction peaks (011) and (101) in pure orthorhombic $SmO_{1-x}F_{1+2x}$ and respectively (0–11), (011), (−101), and (101) in "triclinic" (partly overlapped with (011) and (101) orthorhombic) (the 2θ scale is shifted to align the peaks). (c) Fragment of the phase diagram of the GdOF–GdF_3 system, showing the limits of the orthorhombic (ss2) solid solution and of the "vernier" domain (ss3) (after Ref. (21)).

the "triclinic" phase isolated at low temperature for the same composition in the SmOF SmF_3 system.

In the GdOF–GdF_3 system, the high-temperature metastable phase called *ss*2 by De Kozak *et al.* (21) (Fig. 2c) can also easily be indexed in the orthorhombic system. It is obtained by water-quenching below 750°C and, at 950°C, the limits are $0.30 \leq x \leq 0.36$. They decrease with decreasing temperature ($0.30 \leq x \leq 0.35$ at 900°C; $0.31 \leq x \leq 0.33$ at 750°C).

Comparison of the refined cell parameters of the Nd, Sm, Eu, and Gd phases (Table 1) shows that Sm, Eu, and Gd phases have a similar distortion of the cell parameters by reference to a cubic fluorite phase. The b–a, c/a, and b/a values change only in a limited way.

In contrast, the Nd orthorhombic phase is much less distorted than the others ($b/a = 1.008$–1.009 vs 1.030–1.038) and its composition range is more extended. This confirms that the orthorhombic $NdO_{1-x}F_{1+2x}$ phase has an intermediate character between the tetragonal solid solution stable for higher size Ln cations (La → Nd) and the orthorhombic one stable only from Nd to Gd included.

For Ln cations smaller than Gd, the orthorhombic phase is no longer stable and only the so-called "vernier" phases are isolated in a composition domain closer to MX_2 stoichiometry than the orthorhombic solid solutions which are the subject of the present work.

DEFECT STRUCTURE OF ORTHORHOMBIC $LnO_{1-x}F_{1+2x}$ PHASES

The defect structure of this orthorhombic series has been investigated on powder samples of composition $LnX_{2.33}$ measured on a D5000 Siemens diffractometer under the experimental conditions listed in Table 2.

The average defect structure of $SmO_{0.70}F_{1.60}$ has been used as a model, in space group *Pmmn*. For all phases, the same structural parameters have been refined, with isotropic (for anions) and anisotropic (for Ln cations) thermal

TABLE 2
Refined Structure Parameters for Orthorhombic *Pmmn* $LnO_{1-x}F_{1+2x}$ Phases[a]

	$Nd(O,F)_{2.33}$	$Sm(O,F)_{2.30}$	$Eu(O,F)_{2.33}$	$Gd(O,F)_{2.33}$
		Ln: $2a$ $(\frac{1}{4},\frac{1}{4},z)$		
z	0.2286(1)	0.2267(2)	0.2276(2)	0.2263(2)
β_{11}	0.0100(6)	0.0002(2)	0.0079(8)	0.0029(7)
β_{22}	0.0148(7)	0.0119(4)	0.0213(9)	0.0165(8)
β_{33}	0.0028(3)	0.0010(2)	0.0024(5)	0.0004(4)
$B_{\text{éq}}$ (Å^2)	0.72(4)	0.31(1)	0.83(6)	0.52(5)
		O:$2b(\frac{3}{4},\frac{1}{4},z)$		
z	0.989(3)	0.977(1)	0.980(1)	0.978(1)
B (Å^2)	2.7(2)	1.3(1)	2.1(2)	1.7(2)
		F:$2b$ $(\frac{3}{4},\frac{1}{4},z)$		
z	0.491(3)	0.469(6)	0.461(3)	0.473(2)
τ	0.67(1)	0.53(1)	0.52(1)	0.58(1)
B (Å^2)	2.2(4)	2.1(4)	2.7(8)	3.5(6)
		F″:$4e$ $(\frac{1}{4},y,z)$		
y	0.067(6)	0.097(12)	0.095(5)	0.069(4)
z	0.640(4)	0.617(8)	0.625(3)	0.617(2)
τ	0.33(1)	0.39(1)	0.41(1)	0.38(1)
B (Å^2)	6.2(8)	3.9(4)	4.6(7)	2.8(6)
R_B (%)	2.89	3.32	4.11	3.87
R_P (%)	8.28	8.07	12.69	9.82
R_{WP} (%)	10.46	9.40	15.35	11.51
Program	ARIT4 (37)	ARIT4	FULLPROF (38)	FULLPROF
Angle range (2θ)	15–130	10–143	15–130	15–130

[a] the occupancy parameters $\tau = 1$ for the fully occupied sites.

vibration factors. An example of Rietveld refinement is drawn in Fig. 3. Fourier difference maps are calculated after refinement of the cation and normal anion sites (by reference to fluorite-type structure). They allow one to detect an interstitial site called F″ on a $4e$ $(\frac{1}{4},y,z)$ site. The occupancy factor of all anionic sites has been refined: the O site is quite filled but anionic vacancies exist on the F site and are correlated to the presence of the F″ site, close to the F normal site. The thermal vibration factors of F and F″ sites are rather high which decreases the accuracy of the site occupancy determination. However, all the refinements converge to the same positions and occupancy factors, in perfect agreement with the results of previous studies on many fluorite-related phases. All the interatomic distances agree with the values obtained in homologous phases. Better accuracy would require neutron diffraction experiments, which are impossible with such absorbing *Ln* cations. A bond valence calculation, using Brown's method (25), confirms a O/F order on O and F sites. More details about the refinement process and the main features of these defect structures are reported in the previous papers (5, 24).

Table 2 reports the refined parameters for the four phases. A perfect similarity of the atomic positions is clearly evident between the Sm, Eu, and Gd phases. The interatomic distances (Table 3) show a steady evolution with decreasing ionic radius.

Although isotypic, $Nd(O,F)_{2.33}$ presents significant structural differences from the other phases, in relation with its lower orthorhombic distortion: the normal O and F anions are closer to the homologous positions of the tetragonal high-temperature variety and, therefore, the Nd–O and Nd–F distances are more regular.

In the four phases, the ratio n_{Fi}/n_{VF} (Table 4) is very close to 2, which corresponds in the model previously established (Fig. 4) to the formation of 1:0:2 clusters. These clusters, associating one anionic vacancy in the F layer and two interstitial F″ anions, have been described for the first time in $SmO_{0.70}F_{1.60}$. Their lining up along the $[010]_0$ axis is responsible from the orthorhombic distortion of the fluorite-related lattice (dilation of b and contraction of a cell parameters). The anionic densification only affects the F layers. In all the phases, the thermal vibration factor of F and F″ sites are rather high, which reflects the disordered character of the fluoride sheets. In fact, the 1:0:2 clusters, drawn in Fig. 4c, are likely more irregular on a local scale than this ideal vision. The O planes do not contain any vacancies and remain unchanged, despite the statistical replacement of a great part of the O anions by F ones. These last F anions are likely located in the O sheets at the positions neighboring the F″ interstitial anions of the 1:0:2 clusters. They play an important role in the stability of the defect structure in avoiding too short O–F″ distances.

As above observed, the $b - a$ difference suddenly changes from 0.033 Å for Nd to 0.136 Å for Sm, 0.140 for Eu, and 0.147 for Gd which emphasizes the specific character of Nd in this series. This difference could result either from an incomplete alignment of the 1:0:2 clusters along the b axis, a hypothesis that the structure refinement does not confirm, or from the larger size of the unit cell of the Nd phase which allows the orientation along b of the 1:0:2 clusters without high constraints. This last hypothesis is confirmed by the lack of variation of the cell volume during the orthorhombic–tetragonal transition of the Nd phase. That explains the ease of the reversible transition about 400°C to a tetragonal cell containing 1:0:3 denser clusters (Fig. 4b).

However, the 1:0:2 clusters cannot be considered as completely independent and isolated one from another as the 1:0:3 clusters previously described in many solid solutions, e.g., $Ca_{1-x}La_xF_{2+x}$ (26), $ThO_{2-x}F_{2x}$ (27), $LnN_{0.5-x}F_{1.5x}$ (28), and $LaO_{0.65}F_{1.7}$ (5).

Some arguments tend to show that these 1:0:2 clusters can be associated in higher size units.

The greater extent of the anionic densification, corresponding to juxtaposed 1:0:2 clusters of M_4X_9 composition, is $MX_{2.25}$, much lower than the experimental limit at

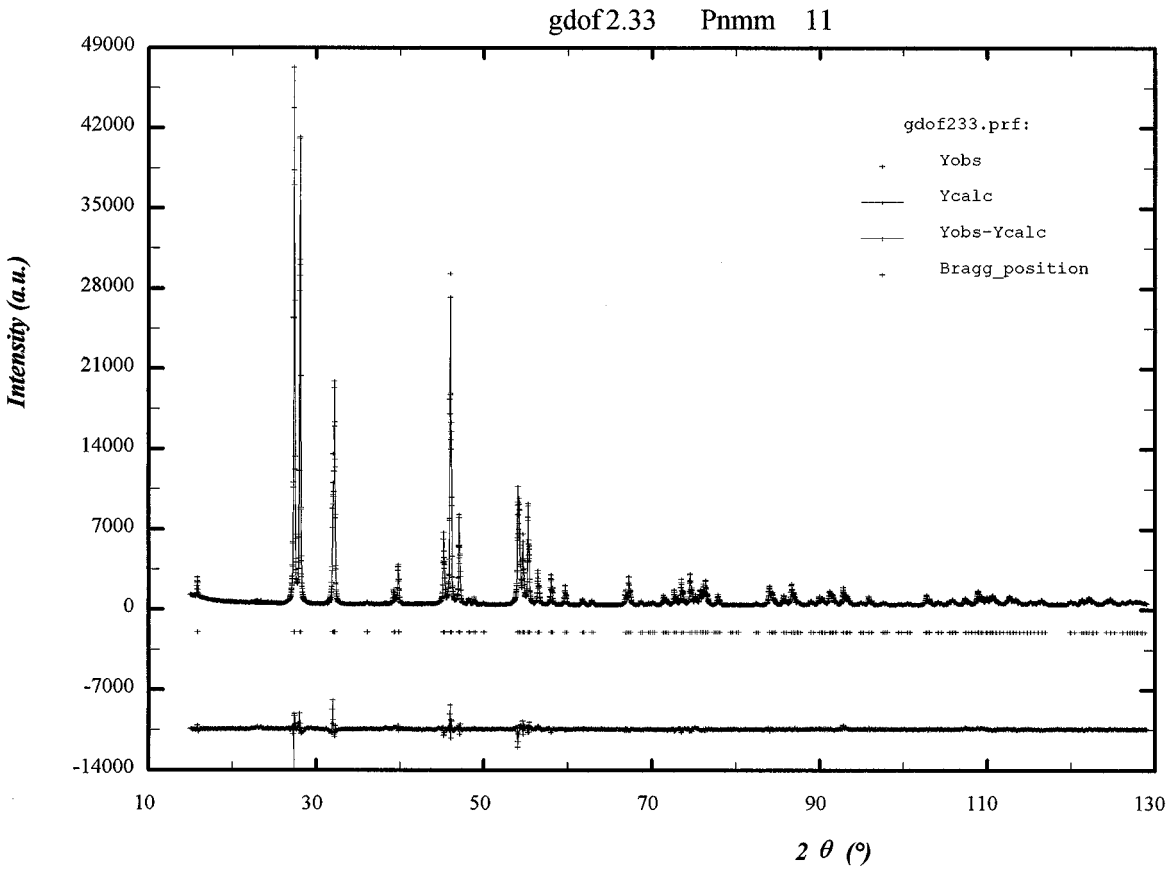

FIG. 3. Rietveld refinement of $GdO_{0.667}F_{1.667}$ in the *Pmmn* space group.

ambient temperature ($\sim MX_{2.35}$). By comparison, the corresponding theoretical limit for 1:0:3 clusters is $MX_{2.50}$, which is almost reached in $Bi(O,F)_{2.45-2.50}$ (29) and $La(O,F)_{2.49}$ (30) for high-temperature metastable varieties presenting some tendency to medium-range or long-range ordering. The tetragonal $LnO_{1-x}F_{1+2x}$ solid solutions are limited to about $MX_{2.4}$.

The presence of a more distorted phase of triclinic symmetry near $MX_{2.35}$ composition tends to show that this composition is close to the physical limit for the accommodation of 1:0:2 clusters in a fluorite matrix.

The following scheme, represented in Fig. 5, can be proposed to explain the defect structure of these orthorhombic

TABLE 3
Main Interatomic Distances in Orthorhombic $Ln O_{1-x}F_{1+2x}$ Phases (Ln = Nd, Sm, Eu, and Gd)

Distances	$Nd(O,F)_{2.33}$ (Å)	$Sm(O,F)_{2.30}$ (Å)	$Eu(O,F)_{2.33}$ (Å)	$Gd(O,F)_{2.33}$ (Å)
Ln_1–O_2	2.419(4)	2.410(3)	2.389(3)	2.381(2)
Ln_1–O_4	2.369(4)	2.323(3)	2.324(3)	2.310(2)
Ln_1–F_2	2.497(6)	2.384(6)	2.343(6)	2.369(5)
Ln_1–F_1	2.574(6)	2.652(7)	2.666(6)	2.616(5)
Ln_1–F_1''	2.49(2)	2.560(8)	2.53(1)	2.47(1)
Ln_2–F_1''	2.46(2)	2.29(1)	2.32(1)	2.30(1)
O_2–O_4	2.839(8)	2.821(5)	2.805(6)	2.794(5)
O_1–F_3	2.851(7)	2.782(11)	2.705(6)	2.764(5)
O_4–F_3	2.861(7)	2.866(11)	2.914(6)	2.829(5)
O_4–F_1''	2.92(2)	2.882(9)	2.85(1)	2.88(1)
O_2–F_1''	2.47(2)	2.69(1)	2.62(1)	2.59(1)
F_1–F_2	2.84(1)	2.831(2)	2.83(1)	2.80(1)
F_1–F_1''	2.29(2)	2.212(9)	2.24(1)	2.22(1)
F_1''–F_2''	2.65(2)	2.81(2)	2.78(3)	2.56(2)

TABLE 4
Comparison of the Experimental Number of Anionic Vacancies V_F and of Interstitial Anions in the F″ Site with the Theoretical Values for 1:0:n Clusters

		n_{VF}	$n_{F''}$	$n_{F''}/n_{VF}$	Theoretical structural formula
Exp	Nd	0.33	0.66	2.0	
	Sm	0.47	0.78	1.7	
	Eu	0.48	0.82	1.7	
	Gd	0.42	0.76	1.8	
Theor	$(2:1:2)_n$	0.667	1.00	1.0	$Ln(O_{1-x}F_x)(F_{1-2x}V_{2Fx})F'_xF''_{2x}$
	$(1:0:2)_n$	0.333	0.667	2.0	$Ln(O_{1-x}F_x)(F_{1-x}V_{Fx})F''_{2x}$
	1:0:3	0.167	0.50	3.0	$Ln(O_{1-x}F_x)(F_{1-x/2}V_{Fx/2})F''_{3x/2}$
	1:0:4	0.11	0.44	4.0	$Ln(O_{1-x}F_x)(F_{1-x/3}V_{Fx/3})F''_{4x/3}$

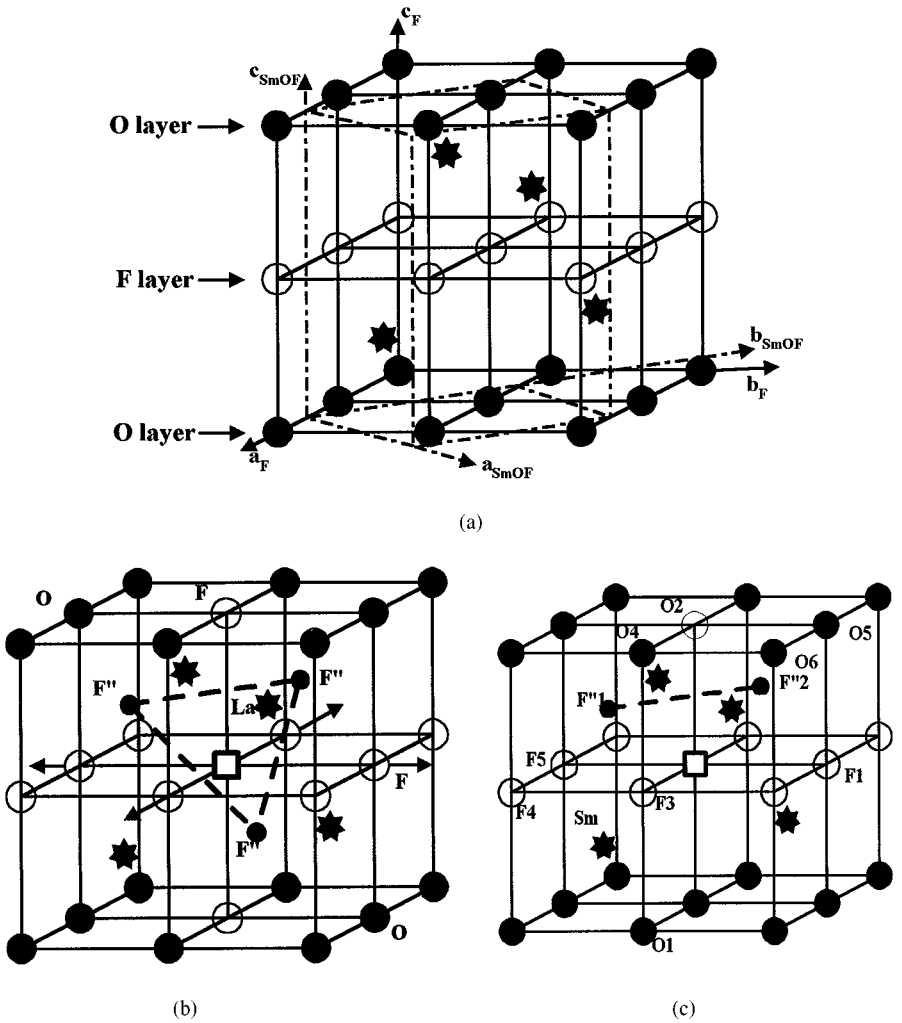

FIG. 4. (a) Orthorhombic unit cell (*Pmmn*) within a cubic fluorite one (*Fm*-3*m*). (b) 1:0:3 and (c) 1:0:2 cluster models for respectively tetragonal $LaO_{1-x}F_{1+2x}$ and orthorhombic $SmO_{1-x}F_{1+2x}$ phases.

oxyfluorides: a 1:0:3 cluster is transformed, by a shift of one X anion, followed by a displacement of a close normal anion in the interstitial X'' position, to two close neighbor 1:0:2 clusters. The structural unit so defined contains six cations, two vacancies, and four X'' interstitial anions. It will be called $(1{:}0{:}2)_2$. Its formula is $Ln_6X_{12-2+4} = Ln_6X_{14}$ or $LnX_{2.33}$ These double 1:0:2 clusters can take several orientations in the fluorite matrix in such a way that long-range disorder can be maintained between the clusters, even for the nominal composition corresponding to a complete juxtaposition of these M_6X_{14} structural units. The coordination of the cations is 8 or 9, in good agreement with the medium size of the *Ln* cations concerned. Moreover, this model allows compositions slightly anion-richer than $MX_{2.33}$. Indeed, it can be imagined, for high densification rates, a progressive lengthening of the structural units by further polymerisation of the 1:0:2 clusters in $(1{:}0{:}2)_3$ linear units, so giving $M_8X_{16-3+6} = M_8X_{19}$ units ($MX_{2.357}$). The formation of longer units should, of course, generate some distortion of the unit cell and formation of microdomains, more or less long-range ordered. That could explain the formation of a triclinic phase at low temperature for compositions close to $MX_{2.35}$. A similar model of clusters becoming progressively longer at high densification rates has already been proposed to explain the partial ordering phenomena inside the $Pb_{1-x}Zr_xF_{2+2x}$ fluorite solid solution (31).

FROM ORTHORHOMBIC SOLID SOLUTIONS TO VERNIER MODULATED PHASES

Vernier phases (Fig. 6c) can be related to fluorite-type structure by a misfit-layer model involving a one-dimensional densification of half the 4^4 anion nets (Fig. 6b),

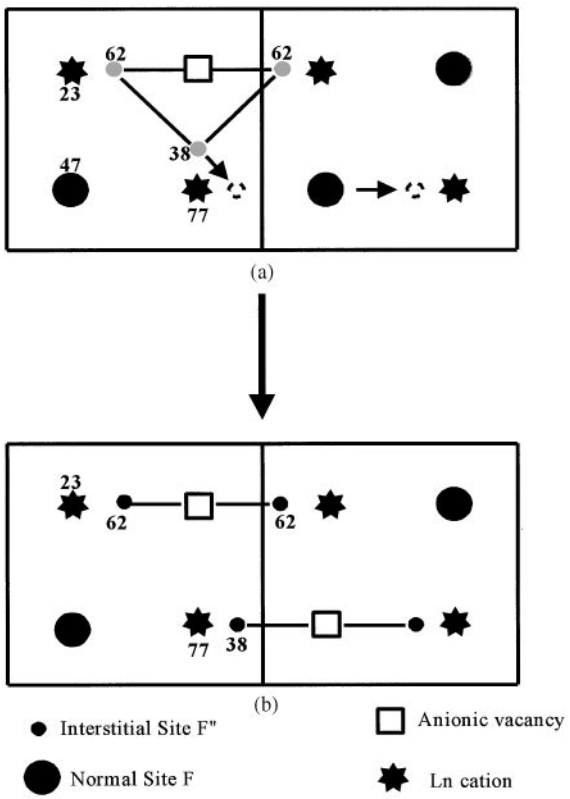

FIG. 5. Proposed mechanism of transformation from a 1:0:3 cluster (tetragonal $NdO_{1-x}F_{1+2x}$) to a $(1{:}0{:}2)_2$ cluster (orthorhombic $NdO_{1-x}F_{1+2x}$) at decreasing temperature.

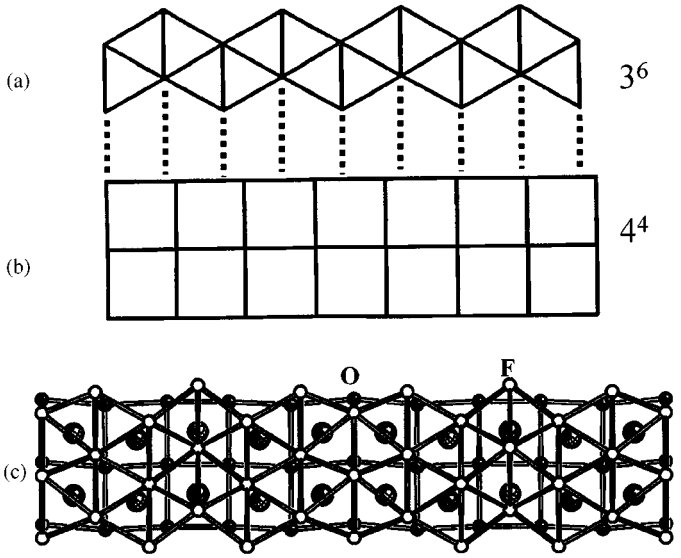

FIG. 6. Vernier phases $Ln_m(O,F)_{2m+1}$. (a) 3^6 hexagonal F layer accommodating the anionic excess. (b) 4^4 square O layer of fluorite type. The dotted lines show the misfit between the two layers. (c) Structure of $Y_5F_7O_4$, a member $m = 5$ of the $Ln_m(O,F)_{2m+1}$ series.

transforming them to denser 3^6 ones (Fig. 6a) (32). This model has been extended using a composite modulated structure approach to these vernier structures (33), considering mutually incommensurate substructures consisting of pseudotetragonal unit layers of XM_4 tetrahedra and pseudohexagonal 3^6 anionic layers, for any composition in the $MX_{2.10}$–$MX_{2.20}$ domain. However, in previous models (20) these phases were described as resulting from an intergrowth of fluorite (or αPbO_2; *m*-ZrO_2) slabs and of densified slabs of structure close to orthorhombic YF_3 type, in proportion varying with composition. Although restricted to the commensurate stoichiometric terms of the M_mX_{2m+1} series, e.g., Bi_3NF_6 and $Lu_3F_5O_2$ (12, 34), and in first approximation to integer *m* values of this series ($Y_5F_7O_4$, $Y_6F_8O_5$, and $Y_{17}F_{23}O_{14}$), this description allows one to focus attention on the densified part of the structure. Figure 7 represents a [100] projection of a fragment of $Y_5F_7O_4$ (Fig. 6c). The anions belonging to the 3^6 anionic net at $x = 0.40$–0.60 related by black connections can be described as $(2{:}1{:}2)_n$ clusters in a defect structure notation. Each (2:1:2) cluster corresponds to three interstitial anions, two in the F″ site and the central one in the F′ site (the vacancy F′ axis is collinear to a $[011]_F$ axis of the fluorite subcell and the vacancy F″ axis to a $[111]_F$ axis). These excess anions flank two anionic vacancies at $x \sim 0$. These clusters are all orientated along the $[001]_F$ direction of the fluorite pseudocell, in contrast with 1:0:2 clusters which are lined up along only one $[011]_F$ direction of this reference cell ($[010]_O$ axis of the *Pmmn* lattice). A $(2{:}1{:}2)_n$ cluster corresponds to the condensation of two $(1{:}0{:}2)_n$ clusters orientated, one along a $[011]_F$ direction and the other along $[01\text{-}1]_F$.

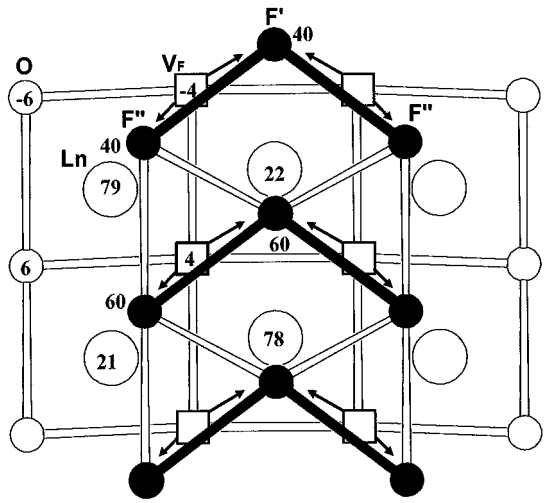

FIG. 7. Identification in the $Y_5F_7O_4$ vernier structure of (2:1:2) clusters (black lines) deriving from (1:0:2) ones by condensation. Their ordered lining up along the $[001]_F$ axis creates YF_3-type slabs.

Structurally speaking, these $(2:1:2)_n$ clusters correspond to slabs of YF_3 type. Associated with contiguous m-ZrO_2 or fluorite slabs, the composition becomes $M_6X_{12-4+6} = MX_{2.33}$. $Lu_3F_5O_2$ and Bi_3NF_6 stoichiometric structures are respectively obtained (35). In the modulated phases, the anionic densification inside the "YF_3" slabs is progressively softened by the modulation of the anionic and cationic fluorite substructure on a variable length along the superstructure direction.

The O/F long-range order in alternate sheets is preserved, perfectly for $Lu_3F_5O_2$ and Bi_3NF_6 and for the most part in the modulated vernier phases, as shown by Papiernik and Frit (36) and Bevan *et al.* (16): as in the phases containing 1:0:2 and 1:0:3 clusters, the densified 3^6 plane net is composed only of F anions and the unmodified square 4^4 plane net is occupied by O anions, except for the site located just below (or above) the $(2:1:2)_n$ cluster (YF_3 slab) above described. This last site is likely occupied by half O and half F anions. This interesting observation perfectly confirms our previous hypothesis concerning the preferential localization of the F anions located in the O sheets at the immediate neighboring of the densified part of the structure (1:0:2 or 1:0:3 cluster) in order to limit the electrostatic repulsion between close O anions about the clusters.

Therefore, the defect structure of the orthorhombic Nd, Sm, Eu, and Gd oxyfluorides has features intermediate between those of the more or less isolated 1:0:3 clusters, stable for tetragonal Ln oxyfluorides with large size *Ln* cations, and the $(2:1:2)_n$ ordered clusters present in the vernier phases, more and more stable for smaller *Ln* cations, and which preserve only a limited freedom of displacement inside the densified planes for the modulated members of this structural series.

The coexistence in the EuOF–EuF_3 and SmOF–SmF_3 systems of an orthorhombic *Pmmn* phase (e.g., $Sm(O,F)_{2.21-2.35}$ at 500°C) and of a vernier domain (e.g., $Sm(O,F)_{2.16-2.19}$) quasi-contiguous or continuous at higher temperature (further work by TEM will be necessary to study the boundary between both domains) suggests that the vernier phases could partly lose at high temperature their modulated character for the medium size *Ln* cations (Sm, Eu). An order–disorder transition involving formation of 1:0:2 clusters by breaking up of the $(2:1:2)_n$ ordered units of the vernier phase seems possible. An examination of the X-ray diffraction patterns of the vernier phases from Lu to Sm shows a progressive weakening of the superlattice reflections. These last reflections are rather weak for Sm and Eu vernier phases. The first explanation for this weakening is a lower distortion of the fluorite subcell for medium size *Ln* cations but it is not impossible to imagine, in the absence of a complete structural study for Eu and Sm vernier phases, that a beginning of disorder can exist with formation of some isolated clusters in addition to microdomains of the modulated perfect vernier structure, especially at temperatures higher than 500–600°C.

CONCLUSION

The series of orthorhombic fluorite solid solutions $LnO_{1-x}F_{1+2x}$, stable for medium size *Ln* cations Sm and Eu, also exist for Nd at low temperature and for Gd at high temperature. Their defect structure is characterized by a change in the clustering of the anionic excess by comparison to the tetragonal solid solutions stable from La to Nd. The dense 1:0:3 clusters are transformed to less dense $(1:0:2)_n$ ones, with a logical decrease of the cationic coordination from 10 + 9 to 9 + 8. The O/F long-range order is maintained.

The vernier phases, more and more stable from Sm to Lu, can be described from a long-range ordering in parallel slabs of $(2:1:2)_n$ clusters, resulting from the condensation of 1:0:2 clusters and structurally equivalent to YF_3-type slabs. The cationic coordination is 8 and 7 in these phases which can be stoichiometric ($Lu_3F_5O_2$) or modulated. The modulation results from the progressive softening, to a variable extent, of the distortion caused by the insertion of these densified slabs. The O/F order in parallel layers is also maintained, perfect in $Lu_3F_5O_2$ and almost perfect in the modulated phases.

The defect structure of the whole series of lanthanide oxyfluorides containing anion excess can therefore be described in a unified way, involving a change in the nature of the clusters, correlated to the progressive decreasing in size of the *Ln* cations. The clusters, free to take many possible orientations in the tetragonal $P4/nmm$ phases, are constrained to line up along one $[010]_F$ axis for orthorhombic *Pmmn* phases and preserve only a one-dimensional degree of freedom in the vernier phases.

For higher densification rates, the organization of the clusters becomes more constrained, which explains the monoclinic distortion of the tetragonal phases (30), the triclinic distortion of the orthorhombic phases, and the existence of a stoichiometric vernier phase $Lu_3F_5O_2$, separated from the modulated vernier domain. The unified character of this structural family is attested by the preservation of the O/F order in parallel sheets. This O/F order constitutes the main feature of all these phases, ordered or not.

REFERENCES

1. W. Klemm and H. A. Klein, *Z. Anorg. Allg. Chem.* **248,** 167 (1941).
2. F. Hund, *Z. Anorg. Allg. Chem.* **265,** 62 (1951).
3. J. Pannetier and J. Lucas, *C. R. Acad. Sci. Paris, C* **268,** 604 (1969).
4. W. H. Zachariasen, *Acta Crystallogr.* **4,** 231 (1951).
5. J. P. Laval, A. Abaouz, B. Frit, G. Roult, and W. T. A. Harrison, *Eur. J. Inorg. Solid State Chem.* **25,** 425 (1988).
6. D. J. M. Bevan, R. S. Cameron, A. W. Mann, G. Brauer, and U. Roether, *Inorg. Nucl. Chem. Lett.* **4**(4), 241 (1968).

7. D. B. Shinn and H. A. Eick, *J. Inorg. Chem.* **8**(2), 232 (1969).
8. A. Abaouz, Ph.D. Thesis, Limoges University, 1989.
9. A. Taoudi, Thesis, Fes University, 1996.
10. A. W. Mann and D. J. M. Bevan, *J. Solid State Chem.* **5,** 410 (1972).
11. D. Roether, Ph.D. Thesis, Albert Ludwigs Universitat Freiburg, 1967.
12. J. P. Laval, A. Taoudi, A. Abaouz, and B. Frit, *J. Solid State Chem.* **118,** 359 (1995).
13. J. H. Müller, T. Petzel, and B. Hormann, *Thermochim. Acta* **298,** 109 (1997).
14. J. Mohyla, Doctoral Thesis, Flinders University, 1979.
15. D. J. M. Bevan and A. W. Mann, *Acta Crystallogr. B* **31,** 1406 (1975).
16. D. J. M. Bevan, J. Mohyla, B. F. Hoskins, and R. J. Steen, *Eur. J. Inorg. Solid State Chem.* **27,** 451 (1990).
17. S. Schmid, *Acta Crystallogr. B* **54**(4), 391 (1998).
18. B. Tanguy, M. Vlasse, and J. Portier, *Rev. Chim. Miner.* **10,** 63 (1973).
19. A. R. Molyneux, Doctoral Thesis, Flinders University, 1971.
20. D. J. M. Bevan and E. Summerville, "Handbook on the Physics and Chemistry of Rare Earths," (K. A. Schneider Jr and L. Eyring, Eds.), Chap. 28, p. 402, North-Holland, Amsterdam, 1979.
21. A. De Kozak, M. Samouël, and A. Chretien, *Rev. Chim. Miner.* **10,** 259 (1973).
22. J. M. Juneja, A. K. Tyagi, G. Chattopadhyay, and S. Seetharaman, *Mater. Res. Bull.* **30**(9), 1153 (1995).
23. J. W. Fergus, *Mater. Res. Bull.* **31**(11), 1317 (1996).
24. J. P. Laval, A. Abaouz, B. Frit, and A. Le Bail, *Eur. J. Inorg. Solid State Chem.* **27,** 545 (1990).
25. I. D. Brown, *in* "Structure and bonding in crystals" (M. O'Keeffe and A. Navrotski, Eds.), Academic Press, New York, 1981.
26. J. P. Laval, A. Abaouz, and B. Frit, *J. Solid State Chem.* **81,** 271 (1989).
27. J. P. Laval, A. Abaouz, B. Frit, and J. Pannetier, *Eur. J. Inorg. Solid State Chem.* **26,** 23 (1989).
28. T. Vogt, E. Schweda, J. P. Laval, and B. Frit, *J. Solid State Chem.* **83,** 324 (1989).
29. J. P. Laval, J. C. Champarnaud-Mesjard, A. Britel, and A. Mikou, *J. Solid State Chem.* **146,** 51 (1999).
30. J. P. Laval and A. Abaouz, to be published.
31. J. P. Laval, C. Depierrefixe, B. Frit, and G. Roult, *J. Solid State Chem.* **61,** 359 (1986).
32. B. G. Hyde, A. M. Bagshaw, S. Andersson, and M. O'Keeffe, *Annual Rev. Mater. Sci.* **4,** 43 (1974).
33. R. L. Withers, S. Schmid, and J. G. Thompson, *Acta Crystallogr. B* **49,** 941 (1993).
34. M. Hofmann, E. Schweda, J. Strahle, J. P. Laval, B. Frit, and M. A. Estermann, *J. Solid State Chem.* **114,** 73 (1995).
35. B. Frit, J. P. Laval, and J. Strähle, *Aust. J. Chem.* **49,** 883 (1996).
36. R. Papiernik and B. Frit, *Acta Crystallogr. B* **42,** 342 (1986).
37. ARIT4: A. Le Bail, H. Duroy, and J. L. Fourquet, *Mater. Res. Bull.* **23,** 447 (1988).
38. FULLPROF: J. Rodriguez-Carvajal, *J. Appl. Cryst.*, to be published.